FISEVIER

Contents lists available at ScienceDirect

Journal of Magnetism and Magnetic Materials

journal homepage: www.elsevier.com/locate/jmmm



Research articles

Lorentz TEM study of the magnetic microstructure in near-eutectoid Co-Pt alloys



Isha Kashyap^a, Eric P. Vetter^b, Jerrold A. Floro^b, Marc De Graef^{a,*}

- ^a Department of Materials Science and Engineering, Carnegie Mellon University, Pittsburgh, PA, United States
- ^b Department of Materials Science and Engineering, University of Virginia, Charlottesville, VA, United States

ARTICLE INFO

Keywords: Magnetic domain wall Eutectoid transformation Lorentz TEM Phase reconstruction

ABSTRACT

In this paper, we report Lorentz Transmission Electron Microscopy (LTEM) observations of magnetic domain structures in a near-eutectoid ${\rm Co_{40}Pt_{60}}$ alloy. The crystallographic microstructure is characterized using conventional bright field/dark field TEM imaging. The magnetic induction orientation inside magnetic domains is extracted from Fresnel through-focus images by reconstructing the phase of electron wave using the transport-of-intensity equation. The alloy shows a nano-chessboard pattern composed of the ${\rm L1_0}$ tetragonal and ${\rm L1_2}$ cubic phases. The magnetization distribution in four neighboring ${\rm L1_0}$ tiles in the nano-chessboard structure is found to follow a vortex/anti-vortex configuration to reduce the magnetostatic and magneto-crystalline anisotropy energies. An unconventional domain wall referred to as an inter phase magnetic domain wall (IPMDW) is observed at the inter-phase boundaries of ${\rm L1_0}$ and ${\rm L1_2}$ phases. Magnetic domain walls in other microstructures (tweed microstructure, macro-twinned structure, coarsened ${\rm L1_0}$ plates) are also documented.

1. Introduction

L1₀-based ordered magnetic alloys, including Fe-Pt, Fe-Pd, and Co-Pt, have long been studied for their applications as hard magnetic materials and in storage devices, primarily due to their high coercivity (H_c) and high energy product ($BH_{\rm max}$) [1–3]. Nano-composite magnetic materials are also increasingly studied in the development of present generation magnetic devices [4–6]. These magnetic alloys usually go through a suitable thermal processing step resulting in optimum microstructures that provide large magnetic anisotropy and high coercivity. One such microstructure is the "nano-chessboard" structure, first discovered by Leroux et al. [7]. Co-Pt alloys with compositions in the narrow eutectoid range around $Co_{40}Pt_{60}$ can undergo a eutectoid transformation via pseudo-spinodal decomposition to produce a unique self-assembled nano-chessboard structure. This microstructure consists of a hard magnetic L1₀ phase (CoPt) and a soft magnetic L1₂ phase ($CoPt_3$), interleaved at the nano-scale.

Co-Pt alloys go through a range of transformations as they are heat-treated to obtain the nano-chessboard structure. First, the eutectoid decomposition transforms a high symmetry FCC disordered phase into two low symmetry ordered phases: $\rm L1_0$ (tetragonal) and $\rm L1_2$ (cubic). This ordering transformation gives rise to various crystallographic boundaries, including anti-phase boundaries (APB), $\rm L1_0$ structural or orientational boundaries and twin boundaries. In addition, the alloy

goes through a paramagnetic to ferromagnetic transformation as it is cooled below the Curie temperature. The ordering of magnetic moments results in the formation of magnetic domains and domain walls. Magnetic domains are coupled to the crystallographic domains through the magneto-crystalline anisotropy energy. Thus, the interplay between crystal domains and magnetic domains dictates the magnetic microstructure and, hence, the magnetic properties. The primary cause for an increased coercivity in L10-type alloys is believed to be magnetic domain wall pinning during the magnetization process [8]. The different crystallographic defects mentioned above can act as pinning centers for the motion of domain walls under the influence of an applied field. However, the degree or extent of pinning varies across various defects. For example, an APB is a weak pinning center whereas a twin boundary is a relatively strong pinning center [9]. From these studies, it is clear that the interaction between magnetic and crystallographic features plays a major role in influencing the magnetic properties. The present work represents an effort to understand the nature of such interactions. A direct characterization of these types of interactions has not been done before at fine length scales of a few nanometers. While there have been reports on the magnetic microstructure studies in Fe-Pd and Fe-Pt alloys, there is little work done on Co-Pt alloys.

Detailed TEM microstructural studies and bulk magnetic properties studies (VSM) of $Co_{40}Pt_{60}$ alloys have been performed by several authors [7,10,11]. Recent work has focused on micro-magnetic

E-mail addresses: epv3cm@virginia.edu (E.P. Vetter), jaf9r@virginia.edu (J.A. Floro), degraef@cmu.edu (M. De Graef).

^{*} Corresponding author.

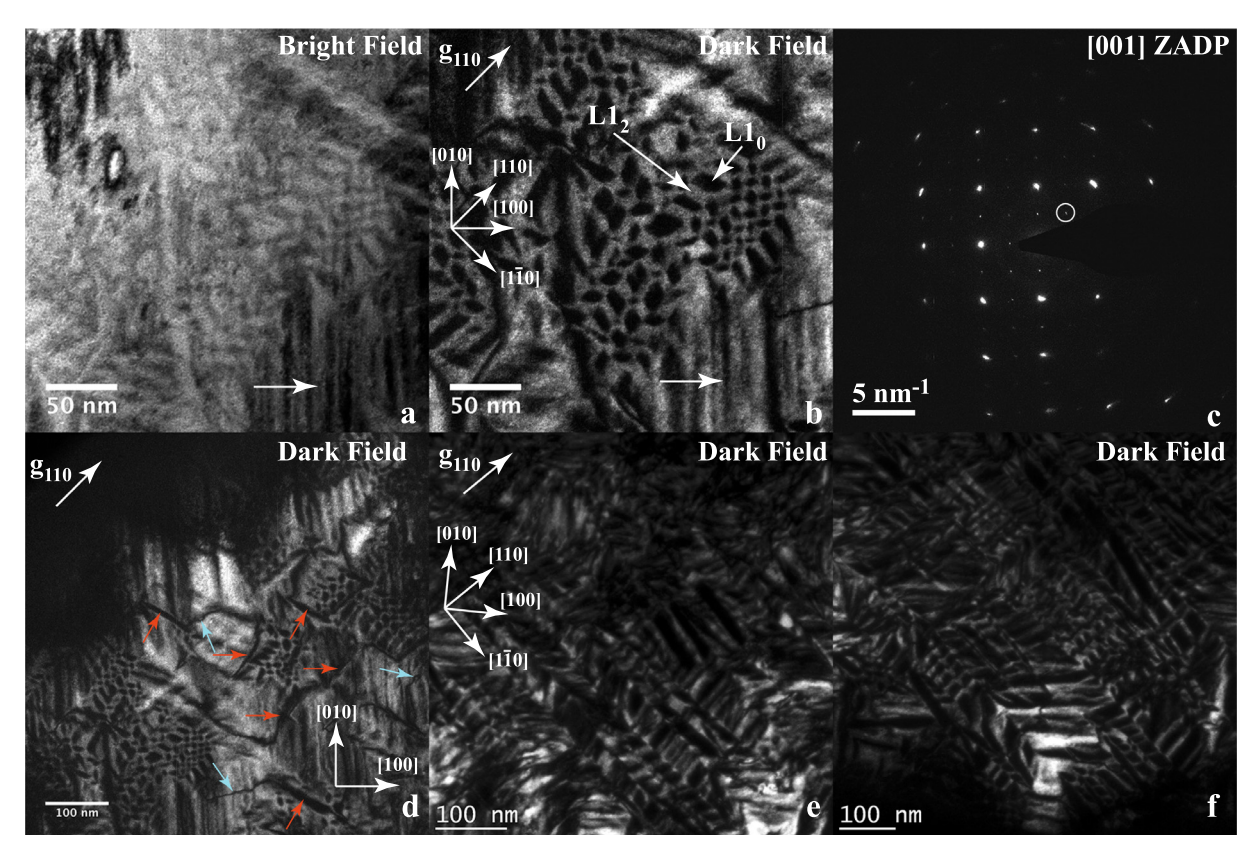


Fig. 1. Conventional TEM images of the nano-chessboard structure. (a) Bright field TEM image, (b) (110) dark field TEM image showing $L1_0$ and $L1_2$ tiles arranged in a nano-chessboard pattern; the relevant crystallographic directions are marked. Solid white arrows in (a) and (b) are pointing to rods corresponding to a nano-chessboard colony along the [010] crystallographic axis, (c) [001] zone axis diffraction pattern of the region imaged in (a) and (b), the directions and planes in diffraction pattern were indexed with respect to the axes of parent cubic lattice A1; the circle indicates the (110) superlattice reflection used for DF imaging, (d) low magnification (110) dark field image of the same region showing multiple nano-chessboard colonies; red arrows point to coarsened $L1_0$ plates while blue arrows point to APBs, (e) and (f) dark field images showing arrangement of coarse $L1_0$ plates within the $L1_2$ matrix.

simulations to understand the length-scale effect of $\rm L1_0-L1_2$ chessboard on the exchange coupling behavior [12]. In a recently published paper [13], we have shown Lorentz TEM image simulation results for the nano-chessboard structure to interpret the various types of magnetic contrast generated by Lorentz TEM imaging. The present paper focuses on the entire range of magnetic microstructures observed in $\rm Co_{40}Pt_{60}$ alloys.

The arrangement of paper is as follows: first, a brief description of the material and the methods used for imaging and data analysis is presented. This is followed by results and discussions. In particular, we show the magnetic domain structure of different crystallographic microstructures observed in $\text{Co}_{40}\text{Pt}_{60}$ alloys; the morphology of magnetic domains and the size/shape of magnetic domain walls is analyzed for each microstructure to establish a relation between the crystallographic microstructure and the magnetic domain structure. The direction of the magnetic induction inside individual magnetic domains is determined from experimental Lorentz through-focus images by reconstructing the phase of the exit electron wave using the transport-of-intensity equation. The effect of the length-scale of the L10 and L12 phases on domain wall formation is discussed in detail. The main conclusions of this work are summarized in the final section.

2. Material and experimental methods

2.1. Co₄₀Pt₆₀ near-eutectoid alloy

The samples analyzed in this study are polycrystalline samples of a $Co_{40.2}Pt_{59.8}$ alloy that were synthesized at the University of Virginia by electric arc melting of high purity Co (99.9%) and Pt (99.99%) in an argon

atmosphere [10,12]. The bulk samples were homogenized at 925 °C for 8 h in a tube furnace and then water quenched to retain the chemically disordered FCC phase. The samples were then slow cooled from 750 °C to 600 °C at a cooling rate of 80 °C per day. Finally, the samples were isothermally annealed at 600 °C for 4 days. Thereafter, TEM thin specimens were prepared by mechanical grinding and dimpling followed by ion milling the samples to electron transparency. X-ray diffraction analysis by [12] shows the co-existence of L10 and L12 phases in this material system. The bulk magnetic properties such as the saturation magnetization (M_s), the coercivity (H_c), and the magnetic energy product ($BH_{\rm max}$) of this alloy are reported to be 4.82 × 10⁵ A/m, 292.2 mT, and 2.6 × 10⁴ J/m³, respectively [12].

2.2. Transmission electron microscopy

Lorentz TEM studies were carried out on an FEI Tecnai F20 field emission transmission electron microscope operated at 200 kV and a FEI Titan 80-300 TEM operated at 300 kV. Both microscopes are equipped with dedicated Lorentz pole pieces that allow for field free imaging of magnetic samples. Additionally, the FEI Titan 80-300 is equipped with a spherical aberration image corrector, which was utilized for high resolution imaging of magnetic domain walls in the nanochessboard structure observed in ${\rm Co_{40}Pt_{60}}$ alloys. Another advantage of spherical aberration correction is that it makes it possible to acquire Fresnel defocused images at low defocus values, which makes the Fresnel images more useful for quantitative analysis. Conventional TEM analysis was performed using the FEI Tecnai F20 microscope. The Fresnel or out-of-focus mode of Lorentz imaging was employed to capture images of magnetic domain walls in this alloy [14]. Phase

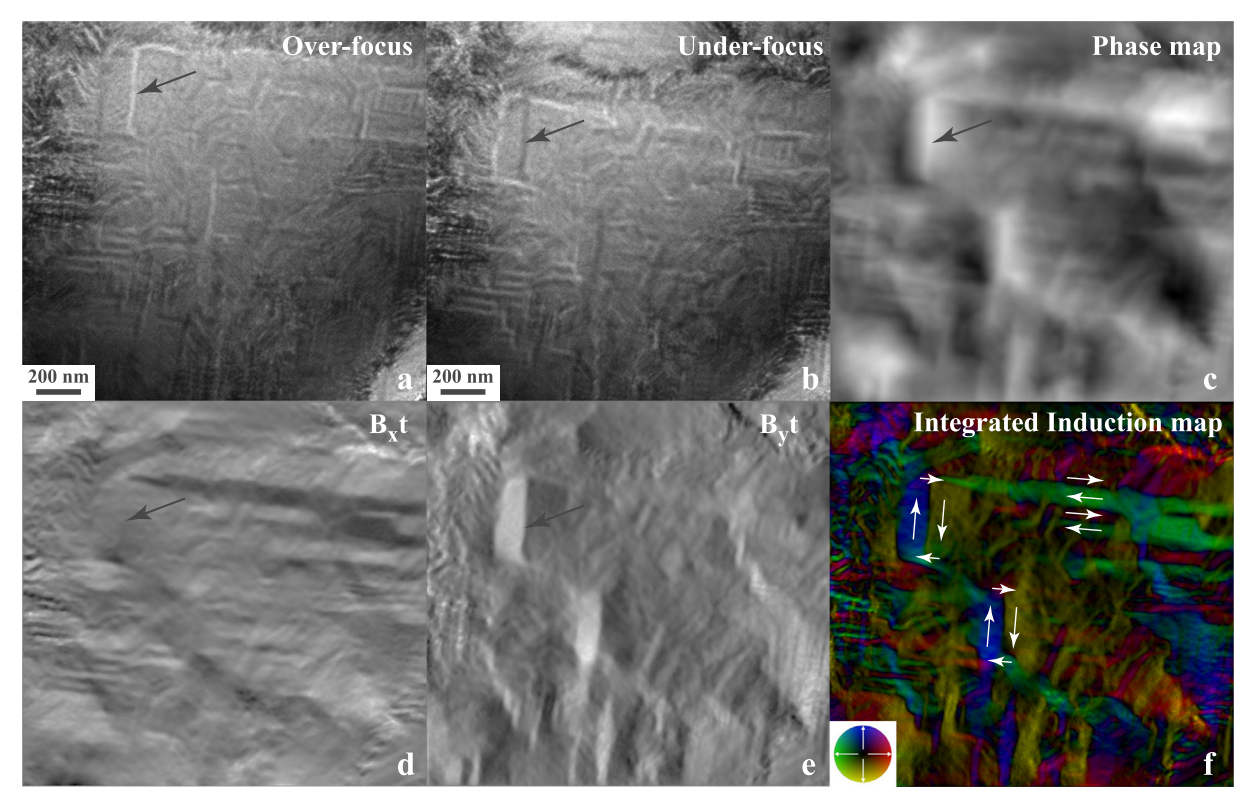


Fig. 2. Lorentz TEM images from a region containing coarse L1₀ plates. (a) Over-focus image ($\Delta f = -7 \,\mu\text{m}$), (b) under-focus image ($\Delta f = +7 \,\mu\text{m}$). The bright and dark lines indicated by black arrows in (a) and (b) correspond to magnetic domain walls; (c) reconstructed phase map, (d) and (e) integrated $B_x t$ and $B_y t$ induction maps, (f) integrated induction color map with the arrows showing the magnetic induction configuration across 180° walls and 90° walls (color legend in inset).

reconstruction based on the transport-of-intensity equation (TIE) was utilized to extract integrated magnetic induction information from the Fresnel through-focus images, as described in detail in [15]. It should be noted that the conventional TEM imaging was performed after the completion of Lorentz TEM experiments, hence it was non-trivial to find the same sample region as used for the Lorentz imaging. However, every effort has been made to correlate similar micro-structural features during the observation and image acquisition process.

3. Results and discussions

3.1. Conventional TEM imaging of the nano-chessboard structure

Fig. 1 shows conventional TEM images of the nano-chessboard structure from a region in the Co₄₀Pt₆₀ alloy. The nano-chessboard structure consists of chessboard colonies that are formed along all three crystallographic axes of the parent cubic grain. When a grain is aligned along one of the crystallographic axes inside the TEM and imaged under the proper diffraction conditions, a perfect nano-chessboard structure is observed. The chessboard colonies along the other two crystallographic axes are seen as parallel rods under this imaging condition. Fig. 1(b) shows one such (110) dark field (DF) TEM image with a nano-chessboard structure containing the L12 phase and two orientation variants of L1₀ phase. Fig. 1(a) is the corresponding bright field (BF) image. All directions and planes in the TEM images and diffraction patterns shown in this paper were indexed with respect to the axes of parent cubic lattice A1 which are retained in L12, and are the axes of the pseudocubic cell of L1₀. The crystal is oriented along the [001] zone axis, as indicated by the zone axis diffraction pattern (ZADP) in Fig. 1(c). The (110) superlattice reflection used for DF imaging has been marked in the ZADP. As can be seen in the DF image, two orientation variants of the $L1_0$ phase are alternating in the [110] and [1 $\bar{1}0$] directions. The $L1_0$ tiles typically have a diamond or parallelogram shape, whereas the L12 tiles are more or less arbitrarily shaped, consistent with earlier results [7,11]. The long axes of the diamond-shaped $L1_0$ orientation variants lie along either the [100] or the [010] axis, in agreement with their respective tetragonal directions. In Fig. 1(a) and (b), the solid white arrows point to parallel rods corresponding to a nano-chessboard colony along the [010] crystallographic axis; these rods are called nanorods. Since the sample is oriented along the [001] zone axis, the rods along the [010] direction are projected as alternating bright/dark contrast in both BF and DF images.

Fig. 1(d) shows a (110) DF TEM image from the same region containing several nano-chessboard colonies. Although this image displays nano-chessboard microstructures with uniform tile size and shape in most instances, several elongated or coarsened L10 plates can also be observed and are indicated by red arrows in the image. This type of L1₀ plates was also reported by Leroux et al. in [7]. They studied Co_{38.5}Pt_{61.5} aged at 700 °C and allowed the sample to go through $L1_2 \rightarrow L1_0 + L1_2$ transformation instead of the A1 \rightarrow L1₀ + L1₂ transformation. This transformation first led to the formation of thin platelets of L10 in the L12 matrix, very similar to the L10 plates shown by red arrows in Fig. 1(d). However, the further evolution of this structure resulted in the formation of thick L10 plates in the L12 matrix with very similar distribution of $L1_0$ and $L1_2$ as in nano-chessboards. The dark field images shown in Fig. 1(e) and (f) also reveal thick plates of L10 decorated in the L12 matrix. Hence, the regions that do not show perfect nano-chessboard structures have gone through slightly different transformations and ordering mechanisms, which may be attributed to compositional inhomogeneity across the sample. Anti-phase boundaries (APBs), indicated by the blue arrows in Fig. 1(d), form another interesting microstructural feature. A detailed analysis of the different types of APBs found in this alloy has been reported previously in [7,11].

3.2. Magnetic domain structure of coarse L10 plates

Fig. 2(a) and (b) show Lorentz Fresnel over-focus and under-focus images from a region of a $Co_{40}Pt_{60}$ alloy. The defocus (Δf) values for each of the out-of-focus images have been specified in the figure caption. The exact orientation of the sample could not be identified because of the limitation of operating the Lorentz TEM in the diffraction mode as there is no suitable lens placed at the back-focal plane of the Lorentz lens. Nevertheless, a relative orientation between different magnetic features can be determined by comparing Lorentz TEM images with the conventional TEM images and electron diffraction patterns of similar regions. The over-focus image in Fig. 2(a) shows a series of magnetic domain walls appearing as white and dark lines apart from the usual diffraction contrast. The under-focus image in Fig. 2(b) has inverted wall contrast, a characteristic of magnetic domain contrast. Note that the over-focus and under-focus images have a slightly different magnification due to the large lens defocus needed to observe the domain walls; the two images are also shifted laterally with respect

The type of magnetic domain arrangement is dependent on the relative orientation of the easy axis of magnetization with respect to the thin foil normal. Straight domain walls in Fig. 2 are indicative of an inplane magnetization direction. The direction of the in-plane integrated magnetic induction was obtained by reconstructing the phase of the exit electron wave from the Fresnel through-focus series; Fig. 2(c) shows the reconstructed phase map. In this map, domain walls correspond to regions where the phase map has curvature, i.e., ridges and valleys. Fig. 2(d) and (e) show the integrated in-plane magnetic induction components $B_x t$ and $B_y t$. The white contrast corresponds to a large induction component along the positive *x*-direction (from left to right), or the positive y-direction (from bottom to top); regions of dark contrast correspond to induction components in the negative x- and y-directions. A color map is generated from the induction component maps, as shown in Fig. 2(f). The color encodes the in-plane magnetization direction defined in the color legend (inset). Several white arrows are overlaid on the color map to show the in-plane magnetization direction for various domains.

Based on the reconstructed phase and color maps, it can be inferred that the domain walls seen in the Fresnel images are 180° and 90° domain walls, since a 180° or a 90° change in color between adjacent domains is observed. Two different magnetic domain morphologies are observed: in the first morphology, the directionality of the magnetic domains, e.g., the large green and red colored rods/plates, strongly indicates that this magnetic region corresponds to a region of coarsened L10 tetragonal variants that seem to have grown from the underlying precursor tweed structure or from the coarsening of the nano-chessboard structure. Since the nano-chessboard formation is strongly dependent upon composition and temperature, a slight deviation in some part of the sample may have resulted in L10 growth instead of nanochessboard growth. Hence, we observe different domain sizes and shapes in the color map. These plate-like domains resemble the coarse L10 plates shown in Fig. 1(d). The coarsening of the nano-chessboard results in the formation of large L10 plates separated by thin regions of L12 phase, as shown in the dark field images in Fig. 1(e) and (f).

The second morphology is a closure-type circular magnetic configuration indicated by white arrows in the color map. This morphology can be seen repeating in this part of the sample. Closure-type magnetic structures are considered to be stable domain configurations since the magnetostatic energy is reduced by minimizing the stray field. However, this structure is mostly observed in materials with more than one easy magnetic axis or in soft magnetic materials, since a closure-type configuration requires a change of magnetization direction. This suggests that these magnetic regions should correspond to the cubic L1 $_2$ phase. However, the comparison with several dark field images similar to Fig. 1(e) and (f) contradicts this interpretation and confirms that the closure-type magnetic regions also belong to L1 $_0$ plates. Within each

closure-type domain structure, the magnetic domain wall separating the two domains (e.g., blue and yellow) appears to lie within the thin strip of L12 phase between the L10 plates. In this case, the magnetization direction of the thin strip of soft L12 phase is completely controlled by the neighboring hard L10 plates, ensuring a smooth transition of magnetization between neighboring L10 plates. The magnetization within domains is oriented along the c-axis or the easy axis of the L1₀ variant. In this case, the green and red domains should correspond to the X-variants of L1₀ phase while the blue and yellow domains should correspond to the *Y*-variants. It should be kept in mind that the Lorentz Fresnel images are acquired for unknown sample orientations, meaning it is possible that the sample may not be oriented along a zone axis: thus, only the in-plane component of the overall magnetic induction is projected in the color induction map instead of the total magnetic induction potentially, giving rise to non-uniform shapes and sizes of magnetic domain contrast. Hence, the shape and size of magnetic domain contrast seen in the Lorentz images may not exactly match with the shape and size of the L10 plates observed in the dark field TEM images.

3.3. Magnetic domain walls in macro-twinned microstructure

Fig. 3 shows Lorentz Fresnel images from a location containing macro-twins. In the in-focus image (Fig. 3(a)), a few macro-twin bands can be observed; white-dashed lines delineate the twin boundaries. Furthermore, macro-twins can be seen comprising fine twins/microtwins with adjacent bands having orthogonal twins. This is known as the polytwin microstructure, a common phase morphology associated with the $A1 \rightarrow L1_0$ transformation [16]. A selected area diffraction pattern obtained in the conventional TEM mode confirmed the presence of twin structure in this sample. In the under-focus image (Fig. 3(b)), magnetic domain walls inside the macro-twins are not clearly visible because of the strong diffraction contrast as well as the fact that the domain walls coincide with the twin boundaries. Another interesting feature in the under-focus image is shown by white arrow. These magnetic features resemble the magnetic contrast due to the nanochessboard structure as will be shown later. However, the spatial resolution of the (uncorrected) Tecnai microscope was insufficient to reveal the magnetic contrast of individual nano-chessboard tiles. The integrated induction color map in Fig. 3(c) shows the in-plane magnetization direction of each of the micro-twins. A magnified view of the marked rectangular area in Fig. 3(c) is shown in Fig. 3(d). It is likely that the sample is not oriented along a zone axis, hence a non-uniform distribution of colors is seen instead of perfectly alternating colors inside the micro-twins. In addition, the color induction map is integrated along the thickness of the sample, which means that all the magnetic domains (randomly oriented) along the sample thickness contribute to the induction map.

$3.4. \ Magnetic \ domain \ walls \ in \ the \ tweed \ microstructure$

In addition to extensive regions comprised of nanochessboard colonies, and less commonly observed areas of coarsened plates or polytwins, another frequently seen structure is shown in Fig. 4. Fig. 4(a) and (b) shows a bright field (BF)-dark field (DF) image pair of the tweed microstructure acquired in conventional TEM mode. The dark field image was acquired using the (100) superlattice reflection in a systematic row beam condition as shown in the inset in Fig. 4(b). Fig. 4(c) shows the [001] zone axis diffraction pattern of this region. The BF-DF image pair clearly shows the tweed contrast along $\langle 110 \rangle$ directions. This contrast is very similar to the tweed microstructure observed in different Fe-Pt [16] and Fe-Pd [8,16] alloys. The images also show a striated contrast of fine plate shaped features along the [100] direction; higher magnification images reveal that these features correspond to the rods of nano-chessboards oriented along [100] crystallographic axis.

Fig. 4(d) and (e) show Fresnel over-focus and under-focus images

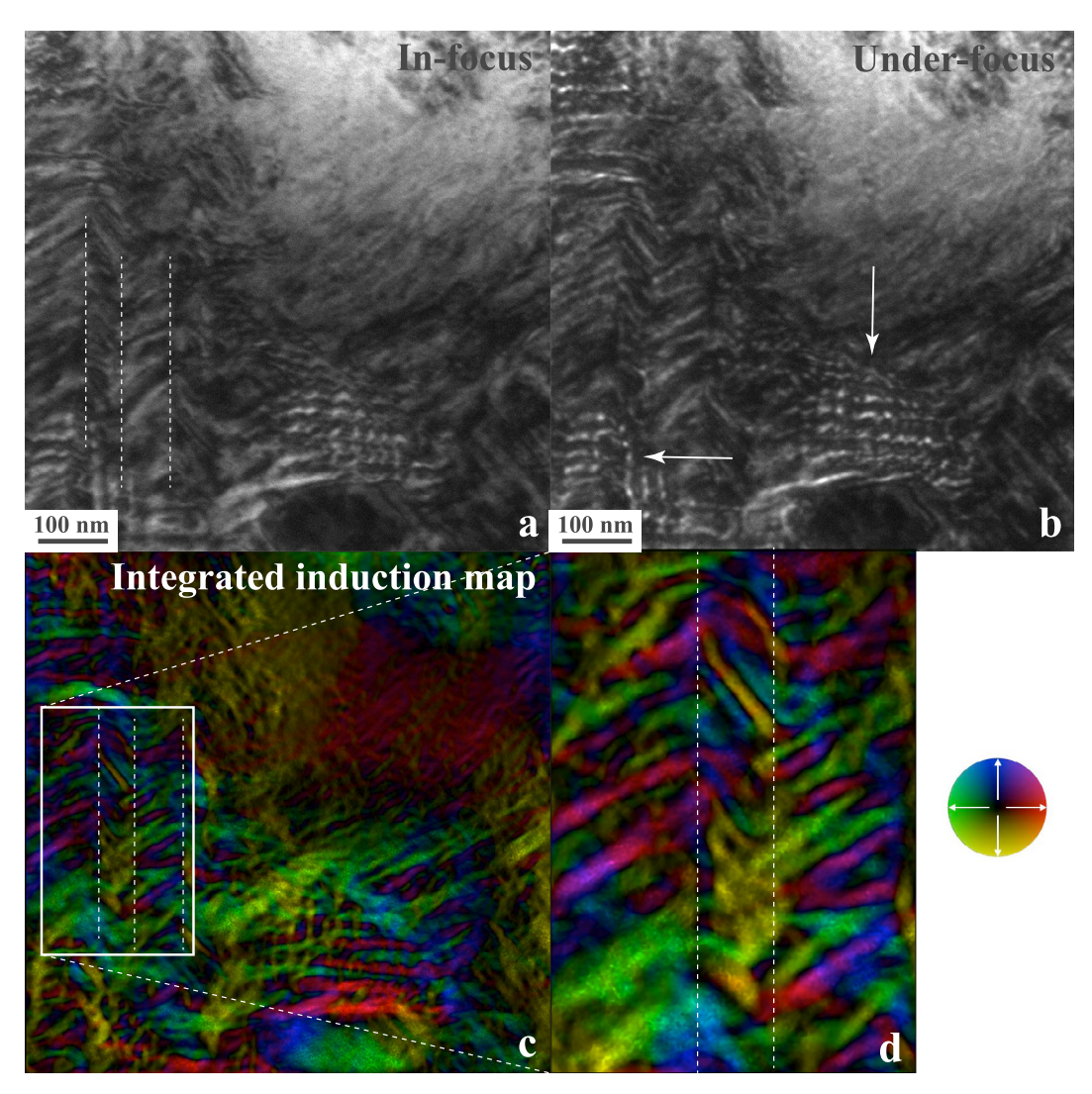


Fig. 3. (a) Lorentz Fresnel in-focus image, white dashed lines indicate twin boundaries, (b) under-focus image ($\Delta f = +1 \,\mu m$), white arrows point to nano-scale fine magnetic features, (c) integrated induction color map, (d) magnified color map of macro-twinned region showing magnetic induction orientation inside fine twins.

from a similar region containing the tweed microstructure. The comparison of the Fresnel images with the BF-DF image pair easily confirms the tweed directions in the Fresnel images. The over-focus image shows tweed contrast in region 1 whereas region 2 shows dark striated features very similar to those observed in the BF-DF pair. Both out-of-focus images show long black and white features in region 1 that resemble 180° and 90° magnetic domain walls; these are magnetic domain walls associated with the tweed microstructure. Similar results were observed by Wang et al. in L10 Fe-Pt alloys [8]. The integrated induction color map in Fig. 4(f) shows the direction of magnetic induction inside the fine L1₀ structural variants. The tweed microstructure/contrast is a result of the relative arrangement of ordered $L1_0$ variants along $\langle 110 \rangle$ directions within the disordered FCC matrix in order to accommodate the lattice mismatch strain produced during ordering; two variants of L10 usually persist as a result of continued annealing. In the case of the eutectoid Co40Pt60 alloy, the tweed microstructure is a result of incomplete transformation of the parent FCC phase into the L10 - L12 nano-chessboard structure. The easy axes of magnetization of the L10 variants are along their c-axes $(M||\langle 100 \rangle)$. Hence, a 90° change in the direction of magnetic induction between adjacent domains can be observed.

The color induction map of region 2 also shows strong magnetic contrast corresponding to nano-rods that consist of two variants of $L1_0$ (X+Y or Y+Z or Z+X) and the $L1_2$ phase. The magnetic contrast in

adjacent nano-rods can be clearly seen in another high magnification image shown in Fig. 5. A grain boundary runs across the middle of Fig. 5(b), indicated by black arrows. On the right of the grain boundary, magnetic domain walls corresponding to the tweed microstructure are visible; on the left, domain walls are associated with nano-rods lying along [100] or [010] axis (assuming an [001] foil normal). The reversal of magnetic contrast can be seen in the under-focus image in Fig. 5(a). The integrated induction color map (Fig. 5(c)) of the marked rectangular area in Fig. 5(b) clearly reveals the fine $L1_0$ magnetic domains. Adjacent L10 variants have their magnetic easy axes perpendicular to each other hence we see a 90° (blue to green or red to yellow) change in magnetization in adjacent L1₀ nano-rods. In addition, the phase shift profile (Fig. 5(d)) of the region marked by a white line in Fig. 5(c) shows the existence of two curved macro domain walls cutting across the nano-rods. Thus, a change in contrast from blue/green to red/ yellow and then again to blue/green is observed. Interestingly, these macro-domain walls are not clearly visible in the out-of-focus images because of overlapping contrast from various domain walls.

3.5. Magnetic domain walls in the nano-chessboard structure

Fig. 6 shows Lorentz images from another region in the $\rm Co_{40}Pt_{60}$ sample acquired using aberration correction in a Titan 80–300 TEM. The over-focus image in Fig. 6(b) shows S-shaped magnetic domain

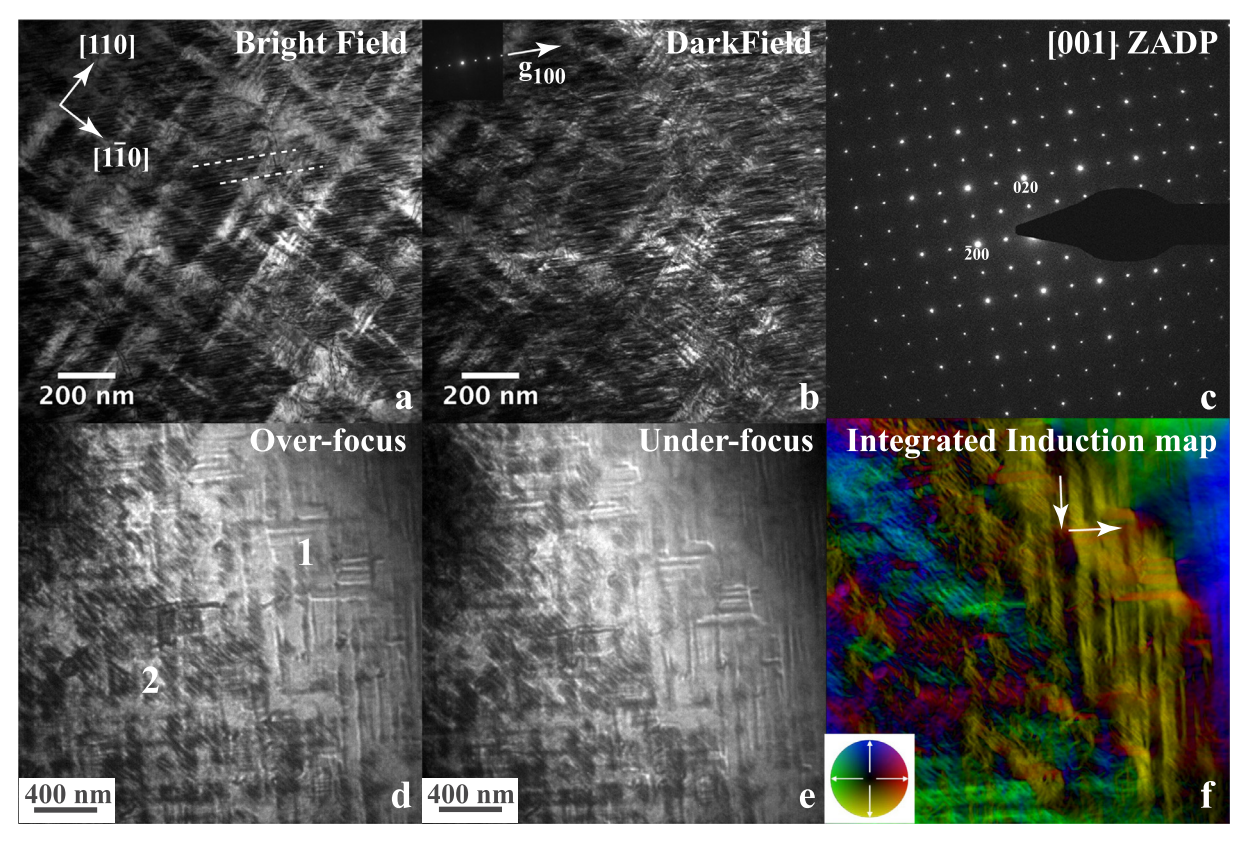


Fig. 4. (a) Bright field image showing tweed microstructure; white dashed lines indicate striated features, (b) dark field image corresponding to (a); inset shows diffraction condition used for imaging, (c) [001] zone axis diffraction pattern, the directions and planes in diffraction pattern were indexed with respect to the axes of parent cubic lattice A1, (d) and (e) Fresnel over-focus ($\Delta f = -4 \,\mu\text{m}$) and under-focus ($\Delta f = +4 \,\mu\text{m}$) image; black and white straight lines are domain walls, (f) integrated induction color map showing various magnetic domains (color legend in inset).

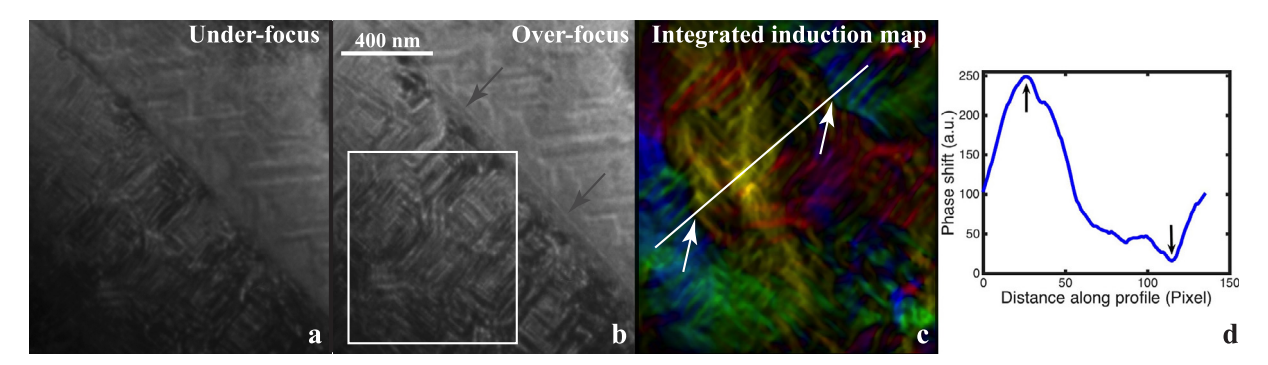


Fig. 5. (a) under-focus image ($\Delta f = +4 \,\mu\text{m}$), (b) Over-focus image ($\Delta f = -4 \,\mu\text{m}$); black arrows point to a grain boundary, (c) magnified image of integrated induction color map of marked rectangular area in (a); white arrows point to macro-domain walls, (d) phase shift profile of line marked in (c).

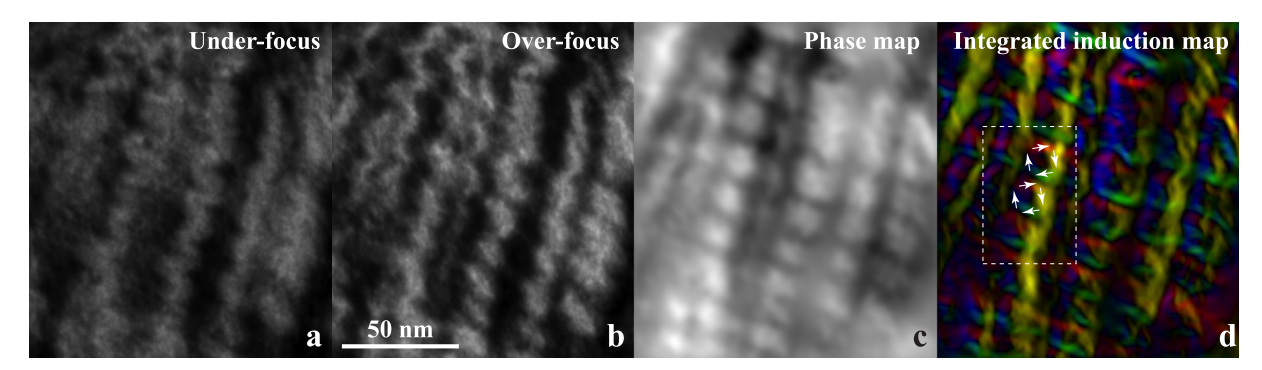


Fig. 6. (a) corresponding under-focus image ($\Delta f = +1 \,\mu m$), (b) Over-focus image ($\Delta f = -1 \,\mu m$) showing zig-zag domain walls, (c) phase reconstructed map, (d) integrated induction color map showing vortex and anti-vortex type magnetic configurations.

walls with white bright contrast; The corresponding under-focus image is shown in Fig. 6(a). The phase map in Fig. 6(c) confirms the position of domain walls. The color magnetic induction map is shown in Fig. 6(d); a repetitive circular magnetization configuration consisting of yellow-red-blue-green color domains can be seen in the color map. This configuration resembles the vortex-type magnetization arrangement observed in many magnetic materials [17–19].

By comparing the Lorentz color map with the conventional dark field TEM images of the nano-chessboard structure shown in Fig. 1(a), it is concluded that the repetitive vortex-type configuration corresponds to different L10 tiles in the nano-chessboard structure. The length-scale of L10 (4 nm to 18 nm) in the DF TEM image match well when compared with the size of magnetic domains in the color induction map. The overlaid magnetization vectors (white arrows) in the color map show the direction of magnetic induction in each of the L10 tiles; each tile is a single magnetic domain whose magnetization points along the easy axes/c-axes of the tetragonal L10 phase. For example, a yellow color corresponds to a $L1_0$ tile whose magnetization lies along [0-10]direction while the neighboring L10 tiles contribute red [100], green [-100], or blue [010] color to the magnetic induction map. The alternating in-plane easy axis in adjacent L10 tiles leads to a vortex-type magnetic configuration that minimizes the overall energy by minimizing both the magneto-crystalline anisotropy energy and the magneto-static energy. The area enclosed in a rectangular box in Fig. 6(d) shows two vortices with an anti-vortex in between; in the phase map, the vortices are bright, and the anti-vortex is dark.

It is not trivial to determine the Curie temperatures (T_C) of the L1₀ and L12 phases in the 2-phase nano-chessboard structure; TEM and VSM studies by Ghatwai et al. [20] on samples with compositions bracketing the two-phase eutectoid region— $Co_{41.7}Pt_{58.3}$ and $Co_{37.6}Pt_{62.4}$ which predominantly contained L10 phase and L12 phase respectively-demonstrated $T_C = 419$ °C for the L1₀ phase and 354 °C for the L1₂ phase. They claimed that these temperatures should also apply to the compositions within the two-phase region and, therefore, to the nano-chessboard structure. Furthermore, the stoichiometric L1₀ CoPt phase is known to have $T_C = 567$ °C [21] whereas stoichiometric L1₂ CoPt₃ has a Curie temperature of $T_C = 15$ °C [22]. Thus, we see that the deviations from stoichiometry significantly affect the value of T_C and thus the magnetic behavior of the alloy. Hence, the Curie temperatures of the individual L1₀ and L1₂ phases of the nano-chessboard in our samples (Co_{40.2}Pt_{59.8}) cannot be predicted accurately. However, it is evident that the L10 phase is largely ferromagnetic at room temperature while the same cannot be said about the L12 phase. The L12 phase could be soft magnetic or paramagnetic at room temperature. In either case, we believe that the magnetization of the L12 tiles is strongly modified/influenced by the surrounding hard L10 tiles due to their close proximity in the nano-chessboard structure. The L12 region essentially acts as a magnetic domain wall (vortex or anti-vortex type) connecting the two $L1_0$ tiles with opposite magnetization; this type of magnetic domain wall has not been reported before. The domain walls that have been reported in the past usually exist within one crystallographic phase [9,8,23]. We propose to call this an inter phase magnetic domain wall (IPMDW). An IPMDW is a domain wall that encompasses a region containing two different crystallographic phases, in this case the L1₀ and L1₂ phases. The formation of an IPMDW is critically dependent on the following factors:

- 1. The two phases should have a coherent interface which ensures that the magnetization transition happens smoothly across the interface.
- One of the phases must to be able to influence the magnetization direction of the other; this happens, for instance, when one of the phases is a strong hard magnetic phase while the other phase is relatively soft.
- 3. The length scales of the individual phases have to be smaller than the critical size for a single magnetic domain particle.

In the case of the Co₄₀Pt₆₀ samples analyzed here, all three conditions are satisfied. The L10 and L12 tiles have been reported [7] to have coherent interfaces in the nano-chessboard structure and the L10 phase is a hard uniaxial magnet while the L12 phase is a soft magnet. In addition, the theoretical single domain particle sizes for L10 and L12 phases were determined to be $\sim 995\,\text{nm}$ and $\sim 75\,\text{nm},$ respectively, using experimentally obtained exchange and anisotropy constants: A(L1₀, L1₂) = $2.5 \times 10^{-11} \text{ J/m}$ and K(L1₀) = $1.5 \times 10^6 \text{ J/m}^3$, K(L1₂) = $2 \times 10^4 \text{ J/m}^3$ [10]. The length-scale measurements show that the sizes of both the $L1_0$ and L12 tiles are well below the respective calculated single domain particle sizes. Hence, no domain wall formation is expected inside the individual tiles. However, the opposite magnetization between two adjacent L10 tiles necessitates the formation of a domain wall between them to minimize the exchange energy, and this is only possible if a domain wall is formed across the L1₂ region between the two L1₀ tiles. In summary, the formation of IPMDWs and vortex-like magnetic configurations in the nano-chessboard structure is a direct result of the balance between the magneto-crystalline anisotropy energy, the exchange energy, and the magneto-static energy which vary rapidly over a length scale of a few tens of nanometers. The domain structure in exchange-coupled, nanocomposite ferromagnets is poorly understood. A model similar to the IPMDW was suggested in [16] for the Co-Pt tweed microstructure, but without the support of domain wall imaging. Here, direct, high-resolution observations of the domain structure in nano-chessboards better motivates and establishes the IPMDW concept.

4. Conclusions

The magnetic domain structure of a near-eutectoid $\text{Co}_{40}\text{Pt}_{60}$ alloy was investigated using Lorentz TEM and conventional TEM imaging. This alloy showed different types of crystallographic and magnetic microstructures as a consequence of the $\text{A1} \rightarrow \text{L1}_0 + \text{L1}_2$ transformation. The typical nano-chessboard structure was observed as a result of the eutectoid transformation; the existence of other microstructures, including tweed, a macro-twinned structure, and coarse L1_0 plates, was attributed to compositional inhomogeneities and annealing conditions across the bulk sample. Anti-phase boundaries due to L1_0 and L1_2 ordering transformations were also observed.

The tweed microstructure is a result of incomplete transformation/ordering and shows a diffuse magnetic contrast associated with the L10 structural variants running along $\langle 110 \rangle$ directions. Several 90° domain walls were observed coinciding with the structural L10 boundaries and a 90° change in direction of magnetic induction between adjacent magnetic domains was observed as the magnetic easy axes of two different L10 variants are perpendicular to each other. Several 90° straight domain walls were observed separating L10 nano-rods of different magnetic orientation; 90° magnetization direction changes between adjacent L10 nano-rods were also found, in addition to curved macrodomain walls cutting across fine nano-rods.

The macro-twinned structure showed several 180° domain walls coincident with the twin boundaries of micro-twins and 90° domain walls lying at the boundaries between macro-twinned plates. The region containing coarsened $L1_0$ plates showed two types of magnetic configurations: rod/plate shaped magnetic domains corresponding to X-variants of the $L1_0$ phase, and circular closure-type patterns encompassing both the X- and Y-variants of $L1_0$ phase. 180° and 90° domain walls were observed separating adjacent $L1_0$ variants.

The nano-chessboard structure revealed the presence of a zig-zag shaped magnetic domain wall which we label as an inter-phase magnetic domain wall (IPMDW) at the inter-phase boundaries between the L10 and L12 phases. The magnetizations in four neighboring L10 tiles are oriented in a closed vortex-type pattern in order to reduce both magnetostatic and magneto-crystalline anisotropy energies. The formation of IPMDWs is likely the result of the inability to nucleate domain walls within the single L10 or L12 phase because of very small length-scale of the nano-chessboard structure.

Acknowledgments

IK and MDG would like to acknowledge financial support from the National Science Foundation, grant DMR-1564550, as well as the Department of Materials Science and Engineering at Carnegie Mellon University. The authors would also like to acknowledge the instrumentation and computational facilities of the Materials Characterization Facility at Carnegie Mellon University under grant # MCF-677785. JAF acknowledges financial support from the National Science Foundation, grant DMR-1709914.

Appendix A. Supplementary data

Supplementary data associated with this article can be found, in the online version, athttps://doi.org/10.1016/j.jmmm.2019.02.036.

References

- [1] J. Coey, Hard magnetic materials: a perspective, IEEE Trans. Magn. 47 (12) (2011)
- [2] B. Zhang, W. Soffa, The structure and properties of L1_0 ordered ferromagnets: Co-Pt, Fe-Pt, Fe-Pd and Mn-Al, Scr. Metall. Mater. 30 (6) (1994) 683–688.
- [3] K. Watanabe, H. Masumoto, On the high-energy product Fe-Pt permanent magnet alloys, Trans. Jpn. Inst. Met. 24 (9) (1983) 627–632.
- [4] R. Skomski, J. Coey, Giant energy product in nanostructured two-phase magnets, Phys. Rev. B 48 (21) (1993) 15812–15816.
- [5] M. McHenry, D. Laughlin, Nano-scale materials development for future magnetic applications, Acta Mater. 48 (1) (2000) 223–238.
- [6] F. Liu, Y. Hou, S. Gao, P. Fazzini, J. Carrey, S. Lachaize, M. Respaud, B. Chaudret, S. Hashimoto, K. Yamada, N. Ohkohchi, L. Manna, M. Salamon, I. Schuller, T. Schulthess, J. Sun, Exchange-coupled nanocomposites: chemical synthesis, characterization and applications, Chem. Soc. Rev. 43 (23) (2014) 8098–8113.
- [7] C. Leroux, A. Loiseau, D. Broddin, G. Van Tendeloo, Electron microscopy study of the coherent two-phase mixtures L1₀ + L1₂, in Co-Pt alloys, Philos. Mag. Part B 64 (1) (1991) 57–82.
- [8] L. Wang, D. Laughlin, Y. Wang, A. Khachaturyan, Magnetic domain structure of Fe-

- 55 at.%Pd alloy at different stages of atomic ordering, J. Appl. Phys. 93 (10) (2003)
- [9] A. Budruk, C. Phatak, A. Petford-Long, M. De Graef, In situ Lorentz TEM magnetization study of a Ni-Mn-Ga ferromagnetic shape memory alloy, Acta Mater. 59 (12) (2011) 4895–4906.
- [10] P. Ghatwai, Structure-property relationships in ordered Co-Pt alloys of near-eutectoid compositions (Ph.D. thesis), University of Virginia, 2015.
- [11] Y. Le Bouar, A. Loiseau, A. Khachaturyan, Origin of chessboard-like structures in decomposing alloys. Theoretical model and computer simulation, Acta Mater. 46 (1998) 2777–2788.
- [12] E. Vetter, L. Geng, P. Ghatwai, D. Gilbert, Y. Jin, W. Soffa, J. Floro, Lengthscale effects on exchange coupling in Co-Pt L1₀ + L1₂ nanochessboards, APL Mater. 4 (9).
- [13] I. Kashyap, Y. Jin, E. Vetter, J. Floro, M. De Graef, Lorentz transmission electron microscopy image simulations of experimental nano-chessboard observations in Co-Pt alloys, Microsc. Microanal. 1–6 (2018).
- [14] M. De Graef, Introduction to Conventional Transmission Electron Microscopy, Cambridge University Press, 2003.
- [15] M. De Graef, Lorentz microscopy: theoretical basis and image simulations, in: M. De Graef, Y. Zhu (Eds.), Magnetic Microscopy and its Applications to Magnetic Materials, Vol. 36 of Experimental Methods in the Physical Sciences, Academic Press, 2000(Ch. 2).
- [16] B. Zhang, M. Lelovic, W. Soffa, The formation of polytwinned structures in Fe-Pt and Fe-Pd Alloys, Scr. Metall. Mater. 25 (1991) 1577–1582.
- [17] A. Petford-Long, M. De Graef, Lorentz microscopy, in: L. Kaufmann (Ed.), Characterization of Materials, Wiley-VCH, 2012, pp. 1787–1801.
- [18] T. Sannomiya, J. Shi, Y. Nakamura, O. Nittono, Correlation between magnetization performance and magnetic microstructure of patterned permalloy films fabricated by microcontact printing, J. Appl. Phys. 96 (9) (2004) 5050–5055.
- [19] S. Venkateswaran, N. Nuhfer, M. De Graef, Anti-phase boundaries and magnetic domain structures in Ni_2MnGa-type Heusler alloys, Acta Mater. 55 (8) (2007) 2621–2636.
- [20] P. Ghatwai, E. Vetter, M. Hrdy, W.A. Soffa, J.A. Floro, Evolution of microstructure and magnetic properties in Co-Pt alloys bracketing the eutectoid composition, J. Magn. Magn. Mater. 375 (2015) 87–95.
- [21] Q. Xiao, E. Brück, Z. Zhang, F. De Boer, K. Buschow, Phase transformation and magnetic properties of bulk CoPt alloy, J. Alloys Comp. 364 (1–2) (2004) 64–71.
- [22] T. Mehaddene, E. Kentzinger, B. Hennion, K. Tanaka, H. Numakura, A. Marty, V. Parasote, M. Cadeville, M. Zemirli, V. Pierron-Bohnes, Lattice dynamics and migration enthalpies in CoPt₃ and FePd, Phys. Rev. B 69 (2) (2004) 024304
- [23] I. Kashyap, M. De Graef, Magnetic domain imaging of Ni-Mn-Ga Heusler alloys using Lorentz TEM, Microsc. Microanal. 22 (S3) (2016) 1720–1721.